Photoionization, Transition Probabilities, and Opacities

Sultana N. Nahar

Department of Astronomy, The Ohio State University
Columbus, Ohio, USA 43210

Abstract. Opacity is a measure of radiation transport through matter. Determination of plasma opacities requires radiative data for bound - bound transitions, the oscillator strengths (f-values), and bound - free transitions, the photoionization cross sections (σ_{PI}), for many levels of the atomic species in all ionization states in the plasma. Hence, large-scale computations are needed to obtain these atomic parameters. Under an international initiative, the Opacity Project (OP), these processes were studied in detail and large-scale ab initio calculations were carried out using the close coupling R-matrix method for the f-values and σ_{PI} of most astrophysically abundant atoms and ions. Application of these data for stellar opacities solved some outstanding problems in astronomy. We have further extended the OP work to electron -ion recombination (the inverse process), unifying the non-resonant and resonant recombination processes, radiative and di-electronic recombination, heretofore treated independently. A theoretically self-consistent treatment of photoionization and recombination is also thereby enabled. In addition, new relativistic calculations using the Breit-Pauli R-matrix (BPRM) method are being carried out under the Iron Project, a second on-going initiative for high-precision studies of collisional and radiative processes of iron and iron-peak elements. The photoionization and recombination cross sections show excellent agreement with recent experiments.

INTRODUCTION

Radiative and collisional atomic processes have been studied in detail through ab initio calculations under two international collaborations, the Opacity Project (OP) (1981-1993) and the Iron Project (IP) (1993-). The Opacity Project [1] was initiated to compute accurate atomic data for the calculation of stellar opacities. Previous astrophysical opacities using existing atomic data led to serious discrepancies with observations of variable luminosity stars - the Cepheid variables and the RR Lyrae. The new opacities substantially increased the contributions of 'metals' (elements heavier than H and He) by factors of two to five in the radiative envelopes, and also solved a number of outstanding problems in the theory of pulsating stars.

The OP work was devoted to radiative processes of the astrophysically abundant

CP547, *Atomic Processes in Plasmas: Twelfth Topical Conf.*, edited by R. C. Mancini and R. A. Phaneuf

elements with Z = 1 - 14, 16, 18, 20, 26 and through their all ionization stages; stellar opacities were obtained using these data.

The aim of the Iron Project [2] is to study electron-ion collisions, as well as radiative processes to higher accuracy than the OP, for iron and iron-peak elements. Whereas the OP calculations assumed LS coupling, the IP work includes relativistic effects in the Breit-Pauli approximation. I will discuss the radiative processes of photoionization, electorn-ion recombination, and bound-bound transitions, investigated under these two projects and their extensions.

PLASMA OPACITIES

The Rosseland mean opacity, κ_R, gives a measure of flow of radiation through a plasma. It is a weighted harmonic mean of the monochromatic opacities, κ_ν, such that

$$\frac{1}{\kappa_R} = \int_0^\infty \frac{1}{\kappa_\nu} g(u) du, \tag{1}$$

where $g(u)$ is the Planck function,

$$g(u) = \frac{15}{4\pi^4} \frac{u^4 exp(-u)}{[1 - exp(-u)]^3}, \quad u = \frac{h\nu}{kT} \tag{2}$$

The monochromatic opacity, κ_ν, depends primarily on (i) the oscillator strength, $f(ij)$, for bound-bound transition of states i and j as

$$\kappa_\nu(i \rightarrow j) = \frac{2\pi^2 e^2}{mc} N_i f(ij) \phi_\nu \tag{3}$$

where N_i is the ion density in state i, and ϕ_ν is a profile factor normalized to $\int \phi_\nu d\nu$ = 1, and ii) on photoionization cross section, σ_{PI}, for the bound - free transitions as

$$\kappa_\nu = N_i \sigma_{PI}(\nu). \tag{4}$$

The total monochromatic opacity, κ_ν, is obtained on summing the contributions from all of the radiative processes, e.g. $f(ij)$ for all possible bound-bound transitions and σ_{PI} of all bound states of all elements present in the plasma and through their ionization stages. Hence accurate determination of opacities require large amount of atomic data.

An example of the complex features of the monochromatic opacity of a single ionization stage of iron, Fe II, is shown in Fig. 1 [3]. The κ_ν spectrum corresponds to a temperature of T = 16000 K and a density of $N_e = 10^{16} cm^{-3}$. The complexity of the spectrum is produced by 19,267 oscillator strengths and photoionization cross sections of 745 bound states of Fe II in LS coupling. The figure shows an enhanced opacity at around u=5.25 ($\approx$ 7.2 eV).

The computations for atomic radiative atomic data under the OP were carried out in the close coupling (CC) approximation using the R-matrix method. The OP raditive data comprise of (i) energy levels, (ii) oscillator strengths and (iii) photoionization cross sections for all astrophysically abundant atoms and ions, and (iv) monochromatic opacities. These are available electronically through OP database system, TOPbase, at the following Website at NASA Goddard Space Flight Center: http://heasarc.gsfc.nasa.gov/topbase/topbase.html, also linked from the Ohio State Website at www.astronomy.ohio-state.edu/~pradhan. It can also be accessed via telnet in the U.S. at topbase.gsfc.nasa.gov or 128.183.101.54, login: topbase pw: Seaton+, and in Europe at 130.79.128.5.

THEORY

The basic methods of the calculations are derived from the atomic collision theory and the close coupling (CC) approximation [4]. The 'ion' core is often referred to as the 'target ion' following the terminology of collision theory. In the coupled channel or CC approximation the wavefunction expansion, Ψ_E, for a total spin and angular symmetry $SL\pi$ or $J\pi$, of the (N+1) electron system is represented in terms of the target ion states as:

$$\Psi_E(e + ion) = A \sum_i \chi_i(ion)\theta_i + \sum_j c_j \Phi_j, \tag{5}$$

where χ_i is the target ion wave function in a specific state $S_i L_i \pi_i$ or level $J_i \pi_i$, and θ_i is the wave function for the (N+1)th electron in a channel labeled as

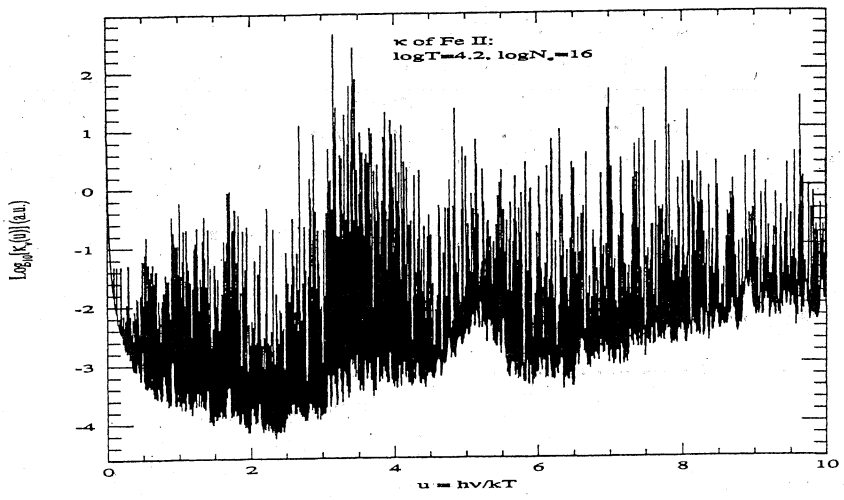

FIGURE 1. Monochromatic opacity, κ_ν, of Fe II
(taken from Ref. [3], with permission from IOP Publishing Ltd.).

$S_iL_i(J_i)\pi_i k_i^2 \ell_i(SL\pi \text{ or } J\pi)$; k_i^2 is the incident kinetic energy. In the second sum the Φ_j's are correlation wavefunctions of the (N+1) electron system that (a) compensate for the orthogonality conditions between the continuum and the bound orbitals, and (b) represent additional short-range correlation that is often of crucial importance in scattering and radiative CC calculations for each $SL\pi$. The complex resonant structures in photoionization and recombination are included through channel couplings.

The non-relativistic (N+1)-electron Hamiltonian for the N-electron target ion and a free electron is

$$H_{N+1} = \sum_{i=1}^{N+1} \left\{ -\nabla_i^2 - \frac{2Z}{r_i} + \sum_{j>i}^{N+1} \frac{2}{r_{ij}} \right\}. \tag{6}$$

Relativistic effects are incorporated into the R-matrix formalism in the Breit-Pauli approximation such that the Dirac equation is reduced to Pauli form with the Hamiltonian

$$H_{N+1}^{\rm BP} = H_{N+1} + H_{N+1}^{\rm mass} + H_{N+1}^{\rm Dar} + H_{N+1}^{\rm so}, \tag{7}$$

where the additional terms are the one-body mass correction term, the Darwin term and the spin-orbit term. The mass-correction and Darwin terms do not break the LS symmetry, and can therefore be retained with significant effect in the computationally less intensive LS calculations. Spin-orbit interaction does, however, split the LS terms into fine-structure levels labeled by $J\pi$, where J is the total angular momentum. The method of inclusion of relativistic effects in the Breit-Pauli approximation is known as Breit-Pauli R-matrix (BPRM) method [2].

At positive energies ($E \geq 0$) the 'channels', characterized by the spin and angular quantum numbers of the (e + ion) system, describe the scattering process with the free electron interacting with the target ion, and the wavefunction, Ψ_F, corresponds to a continuum state. However, at *negative* total energies ($E < 0$) of the (e + ion) system, the solutions of the CC equations occur at discrete eigenvalues of the (e + ion) Hamiltonian that correspond to pure bound states, Ψ_B (all scattering channels are then 'closed').

The positive and negative energy solutions yield many atomic parameters of practical interest: radiative transition probabilities, photoionization and (e,ion) recombination cross sections, electron impact excitation cross sections. The transition matrix elements for these processes are obtained as

$< \Psi_B||\mathbf{D}||\Psi_{B'} >$ $\rightarrow$ oscillator strength,
$< \Psi_B||\mathbf{D}||\Psi_F >$ $\rightarrow$ photoionization and recombination,
$\Psi_F|H(e+ion)|\Psi_{F'} >$ $\rightarrow$ electron impact excitation,

where $\mathbf{D}$ is the dipole operator.

The generalized line strength is calculated from the dipole transition matrix element as

$$S = \left| \left\langle \Psi_f | \sum_{j=1}^{N+1} r_j | \Psi_i \right\rangle \right|^2 \tag{8}$$

which then gives photoionization cross section, σ_{PI},

$$\sigma_{PI} = \frac{4\pi}{3c} \frac{1}{g_i} \omega S, \tag{9}$$

where ω is the incident photon energy in Rydberg units, or the electron-ion recombination cross section, σ_{RC}, which is related to σ_{PI}, as

$$\sigma_{RC} = \sigma_{PI} \frac{g_i}{g_j} \frac{h^2\omega^2}{4\pi^2 m^2 c^2 v^2}, \tag{10}$$

or the oscillator strength, f_{ij}, for the transition between states i and j,

$$f_{ij} = \frac{E_{ji}}{3g_i} S, \tag{11}$$

or the transition probability (A-value) as

$$A_{ji}(s^{-1}) = \frac{1}{2\tau_o} \alpha^3 \frac{g_i}{g_j} E_{ji}^2 f_{ij}, \tag{12}$$

where α is the fine structure constant, and g_i, g_j are the statistical weight factors of the initial and final states, respectively, and $\tau_0 = 2.4191 \times 10^{-17} s$ is the atomic unit of time.

The computational method is based on the powerful R-matrix formalism that enables efficient, accurate, and large-scale calculations of compound (bound and continuum) state wavefunctions of the (e + ion) system at all positive or negative energies. The CC R-matrix computations are extensive and require a number of stages. The R-matrix codes developed for the OP [5] have been extended to BPRM codes [6] to include the relativistic effects in Breit- Pauli approximation. Several extensions of these codes [7,8] are also needed. A schematic diagram of various stages is given in Figure 2. The orbital wavefunctions of the target can be obtained using the atomic structure code SUPERSTRUCTURE [9] which are used as input for STG1 of the BPRM codes. The computational stages, STG1 through STGH, generate the Hamiltonian matrix and the dipole matrix elements for all the symmetries. STGB and STGF create the bound and the continuum wavefunctions respectively. The final results are energy levels, oscillator strengths, collisional, photoionization and recombination cross sections, needed for varied applications.

PHOTOIONIZATION

As mentioned above, the photoionization cross sections including autoionizing resonances are obtained under the OP and the IP. The OP data comprise cross

secitions of about 10^5 bound states of astrophysically abundant atoms and ions. These are being augmented by those being obtained under the IP. For most ions, these cross sections are the first ab initio and detailed calculations.

Fig. 3 shows ground state photoionization cross sections of iron through five ionization stages, Fe I - Fe V [10,3,11–13]. The resonances enhance the background cross sections considerably. Fe IV shows a large resonance structure in the near threshold region. Such complex structures in photoionization of many electron systems are not obtained in simple approximations, i.e. filled squares [14] and dotted curve [15]. For example, the enhanement of the background cross sections is up to three orders of magnitude for Fe I, and over two orders of magnitude for Fe II compared to the earlier calculations.

The CC photoionization cross sections reveal an important feature for excited, valence electron states. Extremely wide resonances, named PEC (photo-excitation-of-core) resonances by Yu and Seaton [16], manifest themselves at photon energies that match the energied of dipole allowed transitions from the target ground state. At this energy, the core is excited while the outer electron remains a spectator, the

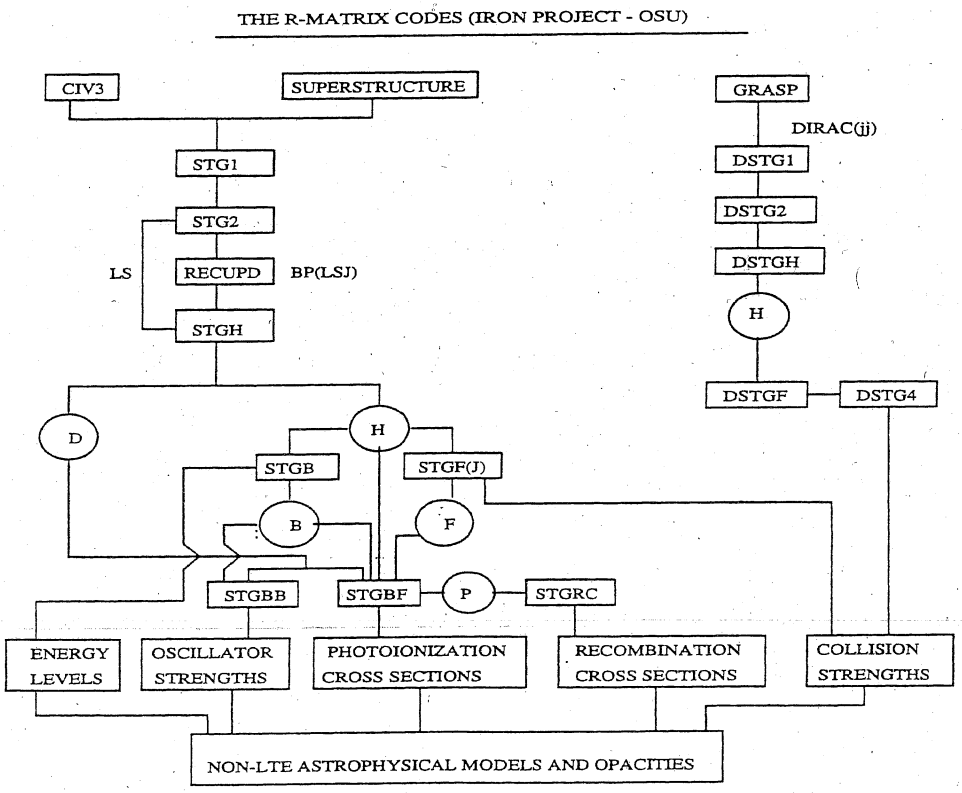

FIGURE 2. Relativistic and Non-relativistic R-matrix codes.

inverse process of dielectronic recombination. In contrast to the typical narrow Rydberg resonances a PEC resonance is wide, and can enhance the background cross section by orders of magnitude. An example is shown in Fig. 4 which presents photoionization cross sections of two highly excited states, $3d^5 8s(^7S)$ and $3d^5 9s(^7S)$, of Fe III [11]. The PEC resonance at the target threshold, $3d^5 4p(^6P^o)$, at about 1.73 Ryd is produced due to the strong $^6S \rightarrow ^6P^o$ dipole transition in the Fe IV core ion

$$h\nu + 3d^5(^6S)ns(^7S) \rightarrow 3d^4 4p(^6P^o)ns(^7P^o) \rightarrow 3d^5(^6S) + e.$$

The PEC resonances are prominent in excited (valence) state photoionization, contradicting the usual assumption of hydrogenic behavior.

Not all these features have been seen experimentally. Recently there have been several very accurate and detailed measurements of photoionization of the ground configuration states (ground state and metastables) of a few atoms and ions. In a recent ion-photon merged beam experiment, Kjeldsen et al. [17] have measured the ground state photoionization cross sections of C II showing extremely rich and detailed resonance structures (Fig. 5). The comparison between the theory [18] and experiment shows excellent agreement, both in terms of magnitude and details of the background and resonances. However, the theoretical calculations were in

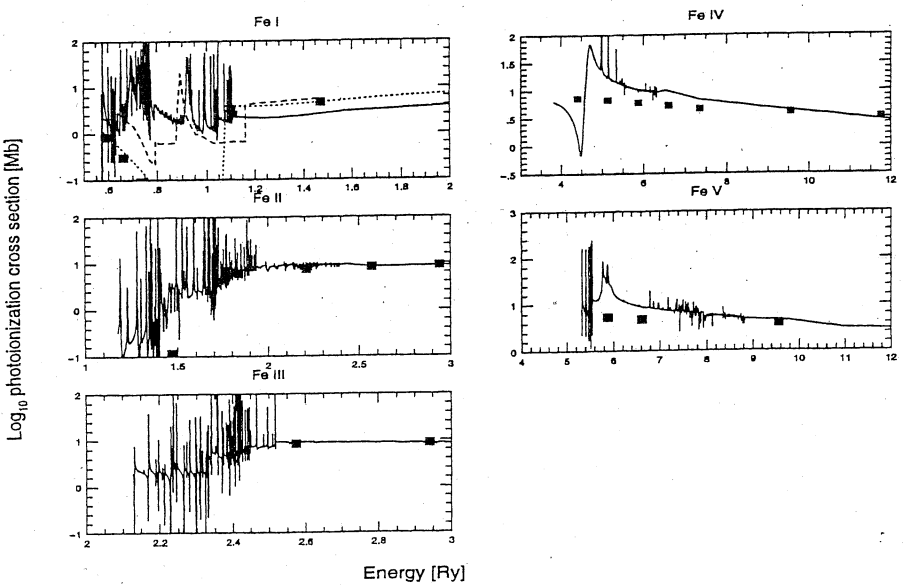

FIGURE 3. Photoionization cross sections for the ground states of Fe I–Fe V including detailed autoionizating resonances (solid curves). Earlier cross sections are solid squares [14] and the dashed curve [15].

LS coupling, neglecting fine structure, that clearly manifests itself in the additional peaks seen in the experimental cross sections (new relativistic calculations are in progress).

Very high resolution measurements of photoionization are being carried out for positive atomic ions at the Advance Light Source (ALS) in Berkeley, where a photon light source is used on an accelerator that produces the ion beams [19]. The first such measurements provide an unprecedented check on theoretical cross sections for the ground and metastable states of O II, particularly resonance structures and fine structure effects (R. Phaneuf and collaborators, private communication).

As the fine structure effects are being observed in experiments, and could be important in the calculation of rates, we are calculating photoionization cross sections using the relativistic BPRM method. Of current interest are the highly charged ions, especially the He- and Li-like ions observed in X-ray sources. Figure 6 presents the σ_{PI} of five levels of Fe XXV, the ground, and the four n=2 levels related to the prominent X-ray K-α lines. The sudden enhancement in the background cross sections at high energies is due to the resonance transition of the core ground level to the n=2 thresholds of Fe XXVI.

ELECTRON-ION RECOMBINATION

Electron-ion recombination is the inverse of photoionization. Although they occur in nature in the same environment, they are usually treated in independent

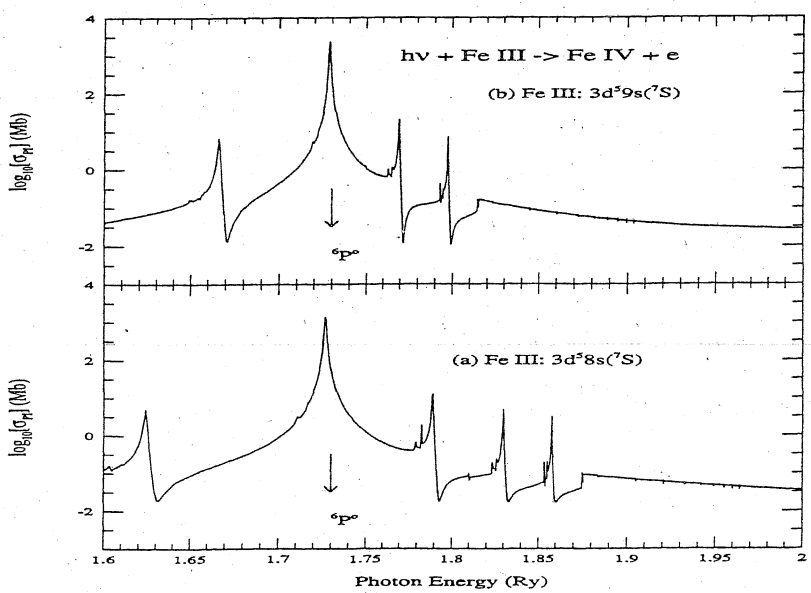

FIGURE 4. Photoionization of excited states of Fe III illustrating the PEC resonance.

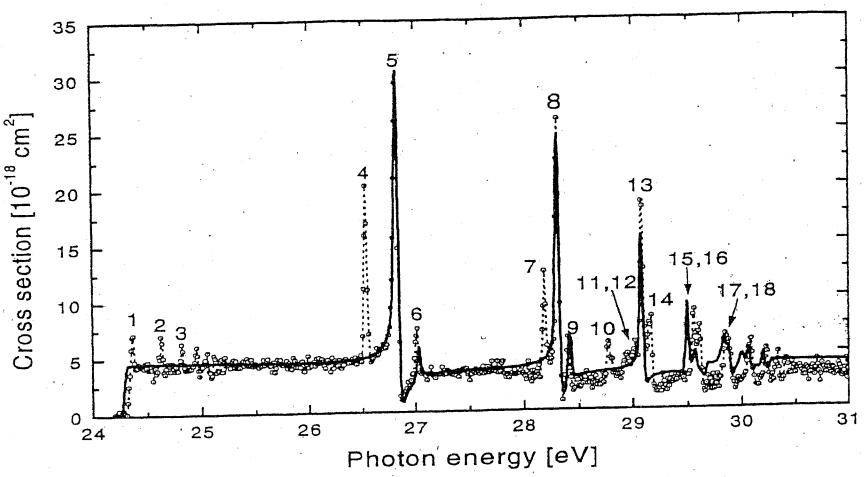

FIGURE 5. Photoionization cross sections of the ground state of C II: experiment (open circle, [17]), theory (solid curve, [18]).

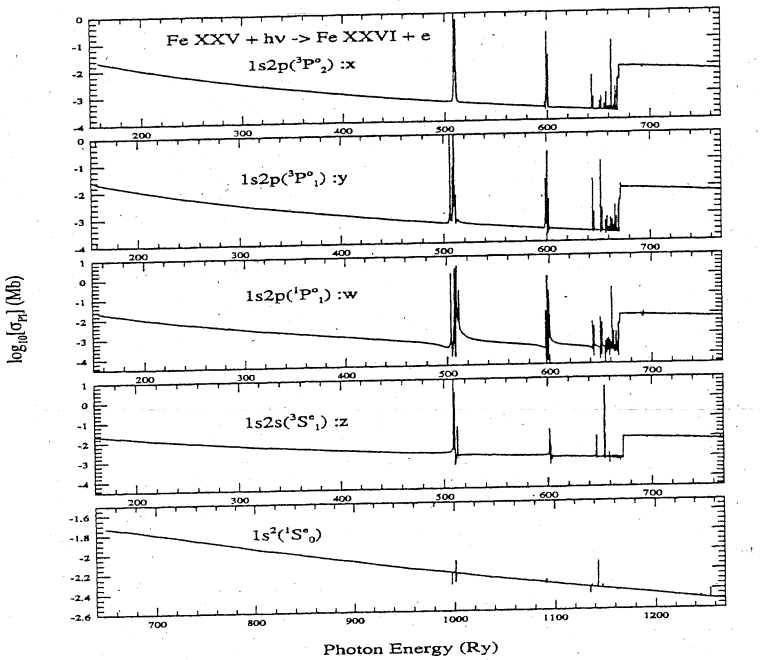

FIGURE 6. Photoionization cross sections of the ground, and n=2 levels that correspond to the K-α lines of Fe XXV.

theoretical frameworks. This introduces a basic inconsistency involving ionization balance in plasmas. We calculate photoionization and recombination cross sections in a self-consistent manner by using the same CC eigenfunction expansions for both processes.

Recombination of an incoming electron to the target ion may occur through non-resonant, background continuum, usually referred to as radiative recombination (RR),

$$e + X^{++} \rightarrow h\nu + X^{+}, \tag{13}$$

which is the inverse process of direct photoionization, or through the two-step recombination process via autoionizing resonances, i.e. dielectronic recombination (DR):

$$e + X^{++} \rightarrow (X^{+})^{**} \rightarrow \begin{cases} (i)\ e + X^{++} \\ (ii)\ h\nu + X^{+} \end{cases}, \tag{14}$$

where the incident electron is in a quasi-bound doubly-excited state which leads either to (i) autoionization, a radiation-less transition to a lower state of the ion and the free electron, or to (ii) radiative stabilization predominantly via decay of the ion core, usually to the ground state, and the bound electron.

Our treatment for electron-ion recombination considers both the RR and DR in a unified manner [7]. These two processes are usually treated separately using different approximations, that may be inaccurate in general since the resonances are inseparable from the background, and the cross sections contain extensive and interacting Rydberg series of resonances (except, possibly, for few-electron, highly charged ions).

The unified treatment for electron-ion recombination is based on the close coupling (CC) approximation using the R-matrix method [20] as used in the OP [4] and the IP [2]. Photoionization cross sections may be computed essentially for all bound states, or levels of excitation $(n, \ell, SL\pi, SLJ\pi)$, energy range, and with resolution of resonances. The cross section for the inverse photo-recombination process is given by detailed balance. However, since recombination takes place to an infinite number of bound states of (e + ion) system, it becomes impractical to do so for the very higly excited levels above a certain n-value (chosen to be 10 in practice). For recombination into levels with n>10, the non-resonant contribution, relative to the resonant contribution per unit energy is negligible owing to the density of resonances as $n \rightarrow \infty$. In that range we employ a precise theoretical treatment of DR based on multi-channel quantum defect theory and the CC approximation [21,7] to compute the recombination cross section.

The unified treatment for recombination is suitable especially for complex ions where channel couplings are strong. The method has been used to calculate the total recombination rate coefficients (α_R) of iron ions, Fe I - Fe V [22–26]. These are presented in Fig. 7 (solid curves). The earlier calculations are the RR rates

(dashed curves) and the DR rates (dot-dashed curves) by Woods et al. [27]. Considerable differences can be noticed between the present unified and the earlier DR results; autoionizations into excited levels in the high temperature region reduces the recombination rates significantly.

These rates together with the self consistent photoionization cross sections will provide more accurate plasma models.

The Rydberg series of resonances in photoionization lead to autoionization in general, especially the low lying ones, as their autoionization rates ($\approx 10^{13--14} s^{-1}$) are several orders of magnitude higher than the radiative rates ($\approx 10^{8--10} s^{-1}$). Hence, radiative decays are not considered for the low n (n$\leq$ 10) resonances for most ions. However, the radiative decay competes with autoionization for highly charged (recombined) ions such He- and Li-like ions. Radiation damping is included for these ions using a perturbative procedure [21,28,8,29]. Fine structure is included in the BPRM approximation.

Very accurate experimental results for recombination cross sections are available for a few ions, mainly He- and Li-like ions, in limited near-threshold energy ranges. However, they are useful for the calibration of theoretical cross sections. Zhang et al [29] have compared in detail the BPRM cross sections with experimental data from ion storage rings for $e + C\ V \rightarrow C\ IV$, $e + C\ VI \rightarrow C\ V$, $e + O\ VIII \rightarrow O\ VII$, with close agreement in the entire range of measurements for both the background (non-resonant) cross sections and resonances. The reported experimental data is primarily in the region of low-energy resonances that dominate recombination (mainly DR) with H- and He-like ions. The recombination rate coefficients, α_R, obtained using the cross sections calculated by Zhang et al. is presented in Fig. 8 where their dotted curve agree closely with those of Savin [30] who used the experimental cross sections to obtain 'experimentally derived DR rates' (dot-long-dash curve). However, Savin's rates do not include contributions

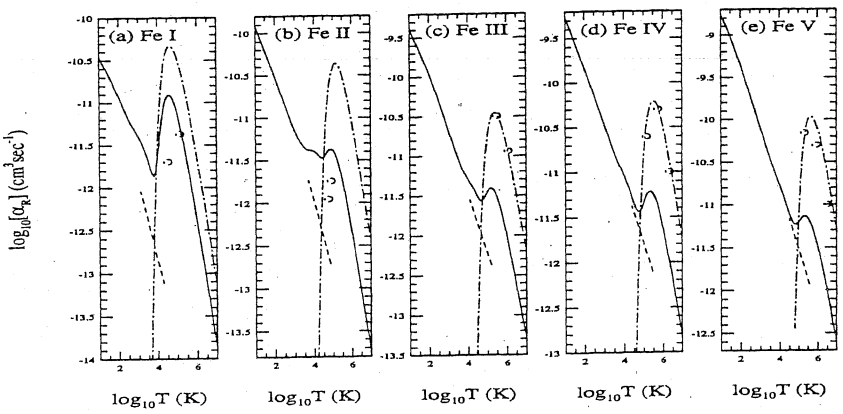

FIGURE 7. Recombination rate coefficients of Fe ions.

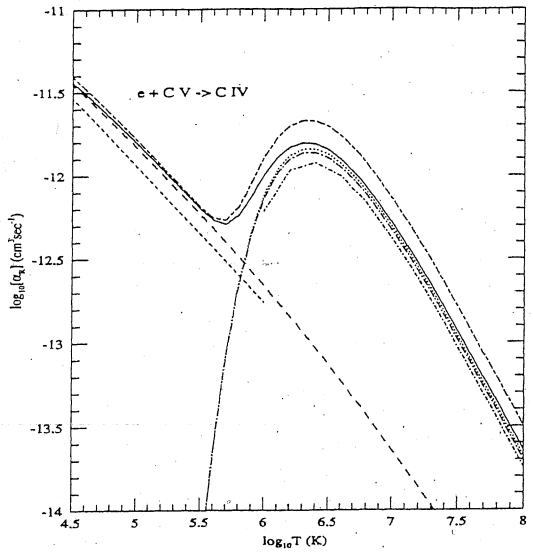

FIGURE 8. Total unified recombination rate coefficients of e + C V → CIV: BPRM with fine structure - solid curve, LS coupling - short and long dashed curve; using cross sections from [29] - dotted; [30] - dot-long dash curve; DR rates: [33] - dot dash curve; RR rates: [34] - short-dash; [35] - long-dash

from much of the low energy non-resonant RR, and very high energy regions. The total unified $\alpha_R(T)$ (solid curve [31]) which includes all possible contributions is, therefore, somewhat higher. The short-and-long dash curve is the total α_R in LS coupling [32] which, at high temperatues, is higher than the new BPRM rates including fine structure and radiation damping (solid curve). The dot-dash curve is the DR rate by Badnell et al [33], which is lower than the others. the dashed and the long-dashed curves are the earlier RR rates [34,35].

TRANSITION PROBABILITIES

The new developments under the IP have enbled calculations of oscillator strengths (f-values), or the transition probabilities (A-values), for dipole allowed as well as intercombination transitions including relativistic effects in Breit-Pauli approximation. The calculations under the OP were carried out in LS coupling. However, since fine structure transitions are needed for analysis of laboratory measurements and for various spectral diagnostics, they have been obtained for a number of atoms and ions, such as Fe II [36], Fe III [37], Fe XIII [38], and other ions, through algebraic transformation of the LS line strengths. These fine structure

transitions correspond to dipole allowed LS multiplets. As they do not include relativistic mixing, the weaker transitions may have larger uncertainties.

The BPRM oscillator strengths are expected to be quite accurate. The oscillator strengths for Fe XXIV and Fe XXV were found to be in excellent agreement with more elaborate calculations including relativistic and QED effects in previous works [39]. One significant advantage of the BPRM method is to enable calculations for a large number of transitions, in contrast to elaborate accurate calculations limited to a few transitions.

The BPRM method is now being applied to complex atoms. In the first such calculation for Fe V [40], we obtain 3865 computed fine structure enery levels, compared to 179 observed ones. These levels correspond to 1.46×10^6 oscillator strengths for the allowed and intercombination E1 transitions. However, a major task has been the identification of these large number of bound fine structure levels in terms of standard spectroscopic designation. The bound levels are initially obtained only as eigenvalues of the (e + ion) Hamiltonian of a given symmetry $J\pi$. Each level therefore needs to be associated with the quantum numbers characterizing a given collision channel. A new scheme, based on the analysis of quantum defects and channel wavefunctions, has been developed [41] to identify the levels with complete spectroscopic information consisting of

$$(C_t\ S_t\ L_t\ J_t\ \pi_t n\ell\ [K]\mathrm{s})\quad J\ \pi. \tag{15}$$

where C_t is the core or the target configuration. The identification scheme also (i) makes correspondence between $SL\pi$ and $J\pi$ designations of levels and (ii) determines the completeness of levels belonging to each LS terms. The purpose is to find all possible bound levels with $n \leq 10, l \leq n-1$, for applications to analysis of experimental measurements and plasma modeling.

Table 1 presents transition probabilities of Fe V of a two multipets, and their fine structure components, with all transitions identified. These belong to a subset of 3727 fine structure transitions among levels that have been observed. The calculated transition energies have been replaced by the observed ones in this set. This subset, as well as the complete dataset of about 1.5×10^6 transitions, is available electronically.

CONCLUSION

We carry out ab initio large scale close coupling R-matrix calculations for (i) bound-bound transition probabilities, (ii) photoionization cross sections, (iii) electron-ion recombination rate coefficients.

The predicted theoretical features in σ_{PI} are being observed in the recent sophisticated experiments. We have self consistent sets of atomic data for photoionization and for its inverse process, electron-ion recombination. Our unified treatment for total electron-ion recombination includes both the radiative and dielectronic

TABLE 1. Transition probabilties of Fe V among observed fine structure levels.

C_i	C_f	$S_iL_i\pi_i$	$S_fL_f\pi_f$	g_i	g_f	E_i (Ry)	E_f (Ry)	f	A_{fi} (s^{-1})
$3d^4$	$-3d^3(4F)4p$	$^5D^e$	$^5F^o$	1	3	5.5132	3.1644	2.154E-01	3.18E+09
$3d^4$	$-3d^3(4F)4p$	$^5D^e$	$^5F^o$	3	3	5.5119	3.1644	3.790E-04	1.68E+07
$3d^4$	$-3d^3(4F)4p$	$^5D^e$	$^5F^o$	3	5	5.5119	3.1496	1.358E-03	3.65E+07
$3d^4$	$-3d^3(4F)4p$	$^5D^e$	$^5F^o$	5	3	5.5094	3.1644	4.617E-02	3.40E+09
$3d^4$	$-3d^3(4F)4p$	$^5D^e$	$^5F^o$	5	5	5.5094	3.1496	5.967E-02	2.67E+09
$3d^4$	$-3d^3(4F)4p$	$^5D^e$	$^5F^o$	5	7	5.5094	3.1443	1.462E-02	4.69E+08
$3d^4$	$-3d^3(4F)4p$	$^5D^e$	$^5F^o$	7	5	5.5058	3.1496	6.895E-03	4.30E+08
$3d^4$	$-3d^3(4F)4p$	$^5D^e$	$^5F^o$	7	7	5.5058	3.1443	5.889E-02	2.64E+09
$3d^4$	$-3d^3(4F)4p$	$^5D^e$	$^5F^o$	7	5	5.5058	3.1496	6.895E-03	4.30E+08
$3d^4$	$-3d^3(4F)4p$	$^5D^e$	$^5F^o$	7	7	5.5058	3.1443	5.889E-02	2.64E+09
$3d^4$	$-3d^3(4F)4p$	$^5D^e$	$^5F^o$	9	7	5.5015	3.1443	1.966E-03	1.13E+08
$3d^4$	$-3d^3(4F)4p$	$^5D^e$	$^5F^o$	7	9	5.5058	3.1391	3.262E-02	1.14E+09
$3d^4$	$-3d^3(4F)4p$	$^5D^e$	$^5F^o$	9	9	5.5015	3.1391	5.139E-02	2.30E+09
$3d^4$	$-3d^3(4F)4p$	$^5D^e$	$^5F^o$	9	11	5.5015	3.1343	7.548E-02	2.78E+09
LS				25	35	5.5055	3.1451	1.068E-01	3.42E+09
$3d^4$	$-3d^3(4F)4p$	$^5D^e$	$^3D^o$	1	3	5.5132	3.1439	5.744E-02	8.63E+08
$3d^4$	$-3d^3(4F)4p$	$^5D^e$	$^3D^o$	3	3	5.5119	3.1439	6.807E-03	3.07E+08
$3d^4$	$-3d^3(4F)4p$	$^5D^e$	$^3D^o$	3	5	5.5119	3.1401	3.147E-02	8.53E+08
$3d^4$	$-3d^3(4F)4p$	$^5D^e$	$^3D^o$	5	3	5.5094	3.1439	4.980E-03	3.73E+08
$3d^4$	$-3d^3(4F)4p$	$^5D^e$	$^3D^o$	5	5	5.5094	3.1401	2.987E-07	1.35E+04
$3d^4$	$-3d^3(4F)4p$	$^5D^e$	$^3D^o$	5	7	5.5094	3.1331	1.149E-02	3.72E+08
$3d^4$	$-3d^3(4F)4p$	$^5D^e$	$^3D^o$	7	5	5.5058	3.1401	6.830E-03	4.30E+08
$3d^4$	$-3d^3(4F)4p$	$^5D^e$	$^3D^o$	7	7	5.5058	3.1331	4.107E-03	1.86E+08
$3d^4$	$-3d^3(4F)4p$	$^5D^e$	$^3D^o$	9	7	5.5015	3.1331	3.671E-03	2.13E+08

recombinations. The self-consistent sets of atomic data for photoionization and recombination should yield more accurate astrophysical photoionization models.

Breit Pauli R-matrix calculations under the Iron Project include (i) dipole allowed and intercombination transitions, (ii) produce large number of accurate f-values, e.g. $\approx$ 1.5 million for Fe V.

ACKNOWLEDGEMENTS

The work has been partialy supported by the NSF and NASA grants.

REFERENCES

1. Seaton M.J., Yu Y., Mihalas D., and Pradhan A.K., *MNRAS* **266**, 805 (1994).
2. Hummer D.G., Berrington K.A., Eissner W., Pradhan A.K, Saraph H.E., and Tully J.A., *A&A* **279**, 298 (1993).
3. Nahar S.N., and Pradhan A.K., *J. Phys. B* **27**, 429 (1994).

4. Seaton M.J., *J. Phys. B* **20**, 6363 (1987).
5. Berrington K.A., Burke P.G., Butler K., Seaton M.J., Storey P.J., Taylor K.T., and Yan Yu., *J. Phys. B* **20**, 6379 (1987).
6. Berrington K.A., Eissner, W., and Norrington P.H., *Comput. Phys. Commun.* **92**, 290 (1995).
7. Nahar S.N., and Pradhan A.K., *Phys. Rev. A* **49**, 1816 (1994).
8. Pradhan A.K., and Zhang H.L., *J. Phys. B* **30**, L571 (1997); Zhang H.L., and Pradhan A.K., *Phys. Rev. A* **78**, 195 (1997).
9. Eissner W., Jone S.W., and Nussbaumer H., *Comput. Phys. Commun.* **8**, 270 (1974).
10. Bautista M.A., and Pradhan A.K., *J. Phys. B* **28**, L173 (1995); Bautista M.A., *Astron. Astrophys. Suppl. Ser.* **122**, 167 (1997).
11. Nahar S.N., *Phys. Rev. A* **53**, 1545 (1996).
12. Bautista M.A., and Pradhan A.K., *Astron. Astrophys. Suppl. Ser.* **126**, 365 (1997).
13. Bautista M.A., *Astron. Astrophys. Suppl. Ser.* **119**, 105 (1996).
14. Reilman, R.F., and Manson, S.T. *Astrophys. J. Suppl* **40**, 815 (1979).
15. Kelly H.P., *Phys Rev A* **6**, 1048 (1972).
16. Yu Yan, and Seaton M.J., *J. Phys. B* **20**, 6409 (1987).
17. Kjeldsen H., Folkmann F., Hensen J.E., Knudsen H., Rasmussen M.S., West J.B., and Andersen T., *Astrophys. J.* **524**, L143 (1999).
18. Nahar S.N., *Astrophys. J. Suppl.* **106**, 213 (1996); *ibid* **101**, 423 (1995).
19. Phaneuf R., Covington, and Aguilar A. (private communication, 1999).
20. Burke P.G., and Seaton M.J., *J. Phys. B* **17**, L683 (1984).
21. Bell R.H. and Seaton M.J, *J. Phys. B* **18**, 1589 (1985).
22. Nahar, S.N., Bautista, M.A., and Pradhan, A.K. *Astrophys. J.* **479**, 497 (1997).
23. Nahar S.N., *Phys. Rev. A* **55**, 1980 (1997).
24. Nahar S.N., *Phys. Rev. A* **53**, 2417 (1996).
25. Nahar, S.N., Bautista, M.A., and Pradhan, A.K., *Phys. Rev. A* **58**, 4593 (1998).
26. Nahar, S.N., and Bautista, M.A., *Astrophys. J. Suppl* **120**, 327 (1999)
27. Woods D.T., Shull J.M., and Sarazin C.L., *Astrophys. J.* **249**, 399 (1981).
28. Sakimoto K., Terao M., and Berrington K.A., *Phys. Rev. A* **42**, 291 (1990).
29. Zhang H.L., Nahar S.N., and Pradhan A.K., *J. Phys. B* **32**, 1459 (1999).
30. Savin D.W., *Astrophys. J.* **523**, 855 (1999).
31. Nahar S.N., Pradhan A.K., and Zhang H.L. (submitted, 2000).
32. Nahar S.N., and Pradhan A.K., *Astrophys. J. Suppl.* **111**, 339 (1997).
33. Badnell N.R., Pindzola M.S., and Griffin, D.C, *Phys. Rev. A* **41**, 2422 (1990).
34. Aldrovandi S.M.V., and Pequignot D., *Astron. Astrophys.* **25**, 137 (1973).
35. Verner D.A., and Ferland G., *Astrophys. J. Suppl* **103**, 467 (1996).
36. Nahar S.N., *Astron. Astrophys.* **293**, 967 (1995).
37. Nahar S.N., and Pradhan A.K., *Astron. Astrophys. Suppl. Ser.* **119**, 509 (1996).
38. Nahar S.N., *At. Data Nucl. Data Tables* **72**, 129 (1999).
39. Nahar S.N., and Pradhan A.K., *Astron. Astrophys. Suppl. Ser.* **135**, 347 (1999).
40. Nahar S.N., Delahaye F., Pradhan A.K., and Zeippen C., *Astron. Astrophys. Suppl. Ser.* **143**, xxxx (2000).
41. Nahar S.N., and Pradhan A.K., *Physica Scripta* **61**, xxxx (2000).